Energy Conversion

DOI: 10.1002/ange.201207277

Nitrogen-Doped Graphene Foams as Metal-Free Counter Electrodes in High-Performance Dye-Sensitized Solar Cells**

Yuhua Xue, Jun Liu, Hao Chen, Ruigang Wang, Dingqiang Li, Jia Qu, and Liming Dai**

Owing to their low-cost production, simple fabrication, and high energy conversion efficiency, dye-sensitized solar cells (DSSCs) have attracted much attention since Oregan and Grätzel's seminal report in 1991.[1] A typical DSSC device consists of a dye-adsorbed TiO_2 photoanode, counter electrode, and iodide electrolyte. The counter (cathode) electrode plays a key role in regulating the DSSC device performance by catalyzing the reduction of the iodide–triiodide redox species used as a mediator to regenerate the sensitizer after electron injection. The ideal counter electrode material should possess a low sheet resistance, high reduction catalytic activity, good chemical stability, and low production costs. Because of its excellent electrocatalytic activity for the iodine reduction, high conductivity, and good chemical stability, platinum has been widely used as a counter electrode in DSSCs. However, the high costs of Pt and its limited reserves in nature have been a major concern for the energy community. Recently, much effort has been made to reduce or replace Pt-based electrodes in DSSCs.[2–11] In particular, carbon black,[5] carbon nanoparticles,[6] carbon nanotubes,[7,8] and graphene nanosheets[3,9–11] have been studied as the counter electrode in DSSCs. However, their electrical conductivities and reduction catalytic activities still cannot match up to those of platinum.

[*] Dr. Y. Xue, Dr. H. Chen, Dr. J. Qu, Prof. L. Dai
Institute of Advanced Materials
for Nano-Bio Applications, School of Ophthalmology
and Optometry, Wenzhou Medical College
270 Xueyuan Xi Road, Wenzhou, Zhejiang 325027 (China)
E-mail: jia.qu@163.com
Dr. Y. Xue, Dr. J. Liu, Prof. L. Dai
Center of Advanced Science and
Engineering for Carbon (Case4Carbon)
Department of Macromolecular Science and Engineering
Case Western Reserve University
10900 Euclid Avenue, Cleveland, OH 44106 (USA)
E-mail: liming.dai@case.edu
Dr. R. Wang, Dr. D. Li
Department of Chemistry, Youngstown State University
One University Plaza, Youngstown, OH 44555 (USA)

[**] This work was supported financially by the AFOSR (grant numbers FA-9550-12-1-0069, FA 9550-10-1-0546, and FA9550-12-1-0037), DOD-Army (grant number W911NF-11-1-0209), US AFOSR-Korea NBIT, UNIST-WCU, NSFC-NSF (grant number DMR-1106160), Case Western Reserve University, Wenzhou Medical College, the Zhejiang Innovation Team from Department of Education (grant number T200917), the Ministry of Education of China (grant numbers IRT1077 and 211069), and the National "Thousand Talents Program" of China.

Supporting information for this article is available on the WWW under http://dx.doi.org/10.1002/anie.201207277.

To improve the device performance for DSSCs with a carbon-based counter electrode, it is important to balance its electrical conductivity and the electrocatalytic activity.[10–12] Since the electrocatalytic activity of graphene for the triiodide reduction often increases with increasing number of defect sites (e.g., oxygen-containing functional groups in reduced graphene oxide),[10] a perfect graphene sheet may have a low charge-transfer resistance (R_{ct}), but a limited number of active sites for catalyzing the triiodide reduction. Unlike chemical functionalization of graphene to introduce electrocatalytic active sites by damaging the conjugated structure in the graphitic basal plan with a concomitant decrease in the electrical conductivity, doping the carbon network with heteroatoms (e.g., N, B, and P) can introduce electrocatalytic active sites with a minimized change of the conjugation length.[13] Furthermore, heteroatom doping has also been demonstrated to enhance the electrical conductivity and surface hydrophilicity to facilitate charge-transfer and electrolyte–electrode interactions, respectively, and even impart electrocatalytic activities.[13,14]

Indeed, our recent articles, along with articles of others, on nitrogen doping of carbon nanotubes and graphene[13–18] have clearly shown that nitrogen-doped carbon nanomaterials can act as metal-free electrodes to show even higher electrocatalytic activities, better long-term operation stability, and more tolerance to crossover/poisoning effects relative to a platinum electrode used for oxygen reduction in fuel cells.[17,18] The newly discovered electrocatalytic reduction activities, together with the doping-enhanced electrical conductivities and surface hydrophilicity, made N-doped carbon nanomaterials ideal as low-cost, but very effective, counter electrodes in DSSCs. To our best knowledge, however, the possibility for N-doped carbon nanomaterials to be used as metal-free electrocatalysts at the counter electrode for triiodide reduction in DSSCs has not been exploited. In the present study, we prepared three-dimensional (3D) N-doped graphene foams (N-GFs) with a nitrogen content as high as 7.6% by annealing the freeze-dried graphene oxide foams (GOFs)[19] in ammonia, and used the resultant 3D N-GFs supported by fluorine-doped tin oxide (FTO) glass substrates as the counter electrode in DSSCs. We found that the resultant DSSCs with the foamlike N-doped graphene counter electrode showed a power conversion efficiency as high as 7.07%, a value which is among the highest efficiencies reported for DSSCs with a metal-free carbon-based counter electrode and is comparable to that of DSSCs with a Pt counter electrode (7.44%) constructed under the same condition. The observed superb performance of DSSCs with the newly developed 3D N-GF metal-free counter electrode can be attributed to the heteroatom doping-induced high

electrical conductivity and good electrocatalytic activity, coupled with the 3D foam structure[2,20,21] with a large surface area, good surface hydrophilicity, and well-defined porosity for enhanced electrolyte–electrode interaction and electrolyte/reactant diffusion.

By annealing the GOF in ammonia (Figure 1a), we produced the first 3D N-GF, though N-doped graphene has been previously produced by various methods, such as in situ chemical vapor deposition (CVD) doping,[16] post-synthesis

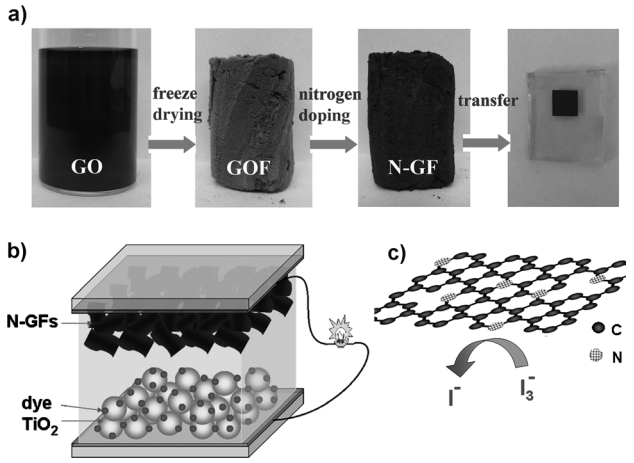

Figure 1. a) Preparation route of the N-GF counter electrode. b) DSSC with an N-GF counter electrode. c) Triiodide reduction on the N-doped graphene surface.

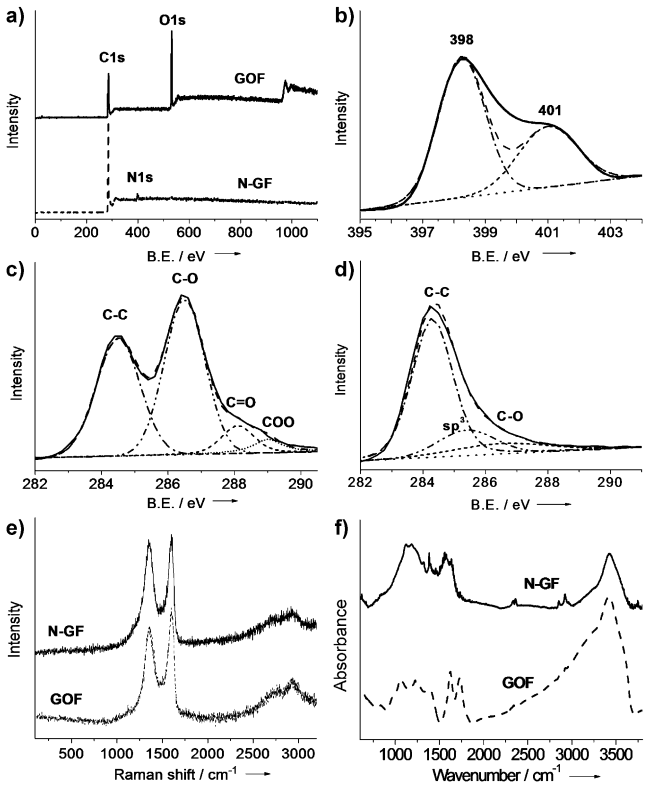

Figure 2. a) X-ray photoelectron survey spectra of GOF and N-GF. b) High-resolution N1s XPS of N-GF. c,d) High-resolution C1s XPS of GOF and N-GF. e) Raman spectra of GOF and N-GF and f) FTIR spectra of GOF and N-GF (B.E. = binding energy).

plasma doping,[22,23] and annealing of the graphene oxide film in nitrogen and ammonia.[24] Most of the previously reported methods for the production of graphene films are often limited to a small production scale and/or the surface doping only. The use of the GOF as a precursor for the post-synthesis annealing in ammonia allows for a low-cost, large-scale production of 3D uniformly N-doped graphene foams, as shown in this work.

The scanning electron microscopic energy-dispersive X-ray (SEM-EDX) mapping images given in Figure S1 in the Supporting Information reveal the uniform distribution for the C, O, and N atoms to confirm that large-scale homogenously N-doped graphene materials have been prepared. To measure the nitrogen content and examine chemical changes caused by the doping with nitrogen, we carried out X-ray photoelectron spectroscopic (XPS) measurements. As expected, the XPS survey spectrum (Figure 2a) for the GOF (see Figures S2 and S3) shows only C1s and O1s peaks at about 285 and 534 eV, respectively. Upon nitrogen doping, a N1s peak appeared at about 400 eV (7.6% N, Figure 2a), accompanied by a significant decrease in the oxygen content because of the reduction of the graphene oxide induced by the doping with nitrogen.[24,25] The high-resolution N1s spectrum of the N-GF shows two peaks at 398 and 401 eV (Figure 2b), corresponding to pyridinic nitrogen and pyrrolic nitrogen, respectively.[26] High-resolution C1s spectra of the pristine GOF before and after doping with nitrogen are given in Figure 2c and d, which show a significant reduction of the C–O peak at 286.5 eV, along with the disappearance of the peaks for the C=O and COO groups because of the reduction of the graphene oxide induced by doping with nitrogen.[24,25] Figure 2e shows the Raman spectra for the GOF before and after doping with nitrogen. As can be seen, the N-GF shows a slightly higher ratio of the peak intensities of the D and G band relative to that of the pristine GOF because of the structural distortion induced by doping with nitrogen, which enhances the electrocatalytic activity of the N-GF counter electrode.[10,27]

Nitrogen doping was further evidenced by the appearance of a C=N bond at 1560 cm^{-1}, which is partially overlapped with the C=C band and a C–N bond at 1385 cm^{-1} in the FTIR spectrum of N-GF (Figure 2f). X-ray diffraction (XRD) profiles for the freeze-dried GOF before and after nitrogen doping have also been recorded (Figure S4). As expected, a pronounced (002) peak at 11.5° was clearly seen for the pristine GOF.[28] In conjunction with the increased I_D/I_G ratio shown in Figure 2e, the shift of the (002) peak from 11.5° for the pristine GOF to 26.2° for the N-GF (Figure S4) indicates that the replacement of relatively bulky oxygen-rich surface groups on the carbon basal plane by nitrogen atoms doped into the carbon network leads to increased structural distortion within the carbon basal plane, whereas the graphitic interlayer spacing is effectively reduced by restacking the reduced graphitic sheets through π-π stacking interactions. The enhanced π-π stacking increased the interaction between the graphene sheets within the N-GF and the mechanical

stability of the N-GF. Removal of oxygen and reduction of space between the layers caused by doping with nitrogen also lead to a significantly increased thermal stability for the N-GF with respect to the pristine GOF (Figure S5).

Figure 3 shows SEM images of the N-GF transferred onto a FTO glass substrate at different magnifications. Figure 3a and b show a foamlike surface structure consisting of flakelike graphene sheets. The side view of the N-GF counter electrode confirmed that the foamlike structure was maintained throughout the entire thickness of the N-GF layer (about 30 μm) on the FTO surface (Figure 3c and d). The graphene oxide material[29] used for the preparation of GOFs contains mainly single-to-a-few layered graphene sheets (Figures S2 and S3). After nitrogen doping of the graphene foam obtained from the freeze-drying process, the thin-layered structure was largely retained in the resultant N-GF (Figure 3 and Figure S6). The high electroactive surface area of the N-GF (BET: 436 $m^2 g^{-1}$; see Figure S7) should enhance the contact between the N-GF counter electrode and the I^{3-}/I^- electrolyte solution in the DSSCs. Figure 1a shows a photodigital image of a FTO glass counter electrode of 0.5 × 0.5 cm^2 coated with the N-GF. Figure 1b illustrates schematically the structure of a DSSC with a N-GF-coated FTO glass as the counter electrode. For comparison, platinum and other relevant materials were also used as the counter electrode in DSSCs constructed under the same condition in control experiments.

The device performance for DSSCs with N-GF, reduced graphene oxide foam (rGOF), spin-coated N-doped graphene (N-graphene) film, spin-coated rGO film, and platinum, respectively, as the cathode was measured. Figure 4a shows the representative current density–voltage characteristics with the numerical data listed in Table 1. As can be seen, the Pt-based reference DSSC exhibited a short circuit current (J_{sc}) of 14.27 mA cm^{-2}, an open circuit voltage (V_{oc}) of 0.79 V, a fill factor (FF) of 0.66, and an overall power conversion efficiency of 7.44%. The DSSC with the N-GF counter electrode showed an even higher J_{sc} of 15.84 mA cm^{-2} and an V_{oc} of 0.77 V, but a lower FF of about 0.58, and a power conversion efficiency of 7.07%. By contrast, the J_{sc}, V_{oc}, FF, and power conversion efficiency for the DSSC with the rGOF as counter electrode are only 14.34 mA cm^{-2}, 0.75 V, 0.45, and 4.84%, respectively. These data clearly indicate the important role of the nitrogen doping for the carbon-based metal-free counter electrode in DSSCs. As can be seen in Figure 4a, the N-GF counter electrode exhibited a similar performance as the Pt counter electrode, both outperformed the rGOF counter electrode. Figure 4a and Table 1 also indicate that the performances of graphene foams (i.e., N-GF and rGOF) are much better than the corresponding spin-coated graphene films (i.e., N-graphene and rGO films). Therefore, it is the combined effect of nitrogen doping and foamlike structure that endows the N-GF counter electrode with a superb performance. Besides, Figure 4b shows the incident photon to

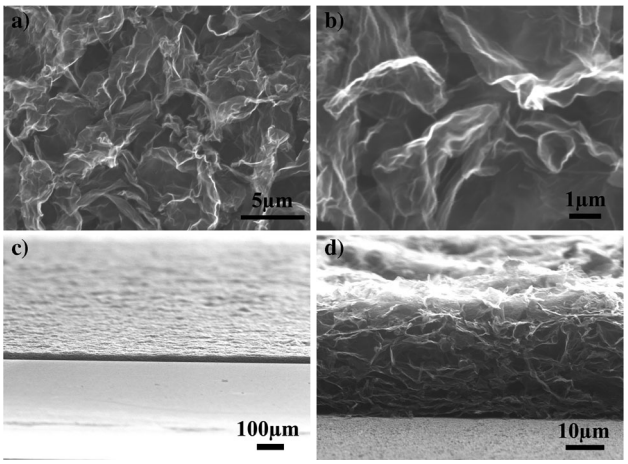

Figure 3. a,b) Top-view SEM images and c,d) side-view SEM images of the prepared N-GF counter electrode at different magnifications.

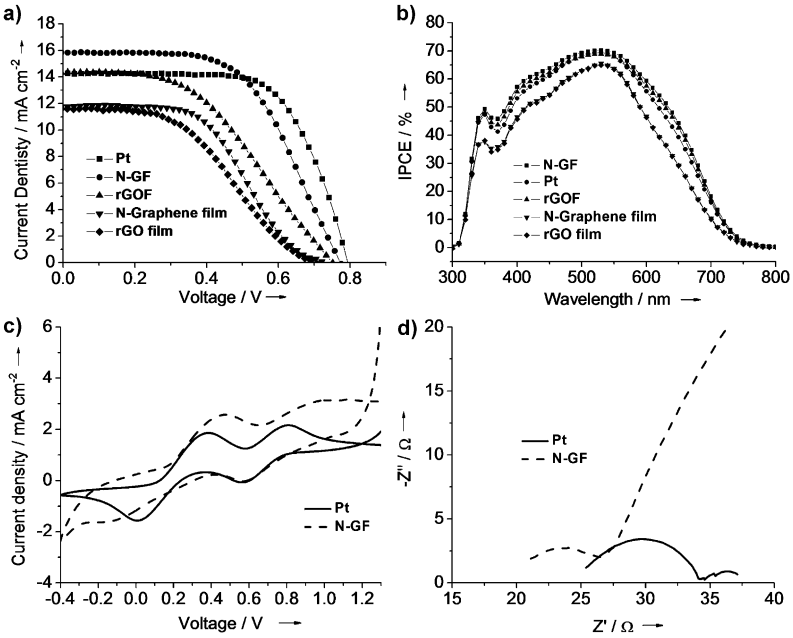

Figure 4. a) Current density–voltage characteristics and b) incident photon to charge carrier efficiency (IPCE) of DSSCs with Pt, N-GF, rGOF, N-graphene film, and rGO film counter electrodes. c) Cyclic voltammograms of N-GF and Pt on a FTO glass substrate cycled in the I^-/I_3^- electrolyte (10 mM LiI + 1 mM I_2 + 0.1 M $LiClO_4$ + acetonitrile) at a scan rate of 50 mV s^{-1}. d) Nyquist plots of symmetric dummy cells with a Pt and N-GF counter electrode.

Table 1: Short circuit current (J_{sc}), open circuit voltage (V_{oc}), fill factor (FF), and power conversion efficiency for DSSCs with N-GF, rGOF, N-graphene, rGO film, and Pt as counter electrodes, respectively.

Counter electrode	J_{sc} [mA cm^{-2}]	V_{oc} [V]	FF	Efficiency [%]
Pt	14.27	0.79	0.66	7.44
N-GF	15.84	0.77	0.58	7.07
rGOF	14.34	0.75	0.45	4.84
N-graphene film	11.75	0.73	0.49	4.20
rGO film	11.60	0.70	0.43	3.49

charge carrier efficiency (IPCE) for DSSCs with N-GF, rGOF, rGO, N-graphene, and Pt counter electrodes, respectively. As expected, the foamlike electrodes (N-GF and rGOF) show relatively high IPCEs compared to their film-type counterparts (i.e., N-graphene and rGO films).

To better understand the improved DSSC performance for the N-GF counter electrode, we measured cyclic voltammograms (CVs) of the I^-/I_3^- redox couple on both the N-GF and Pt electrodes, and obtained similar CV curves with two pair redox peaks. The relatively negative pair can be attributed to redox reaction (1), whereas the more positive pair is assigned to the redox reaction (2). The relatively high anodic and cathodic peaks observed for N-GF with respect to the Pt electrode suggest a high electrocatalytic activity for the reduction of triiodide ions at the N-GF electrode, as previously demonstrated for N-doped graphene and carbon nanotubes for the oxygen reduction reaction.[16,18]

$$I_3^- + 2e^- \rightarrow 3I^- \quad (1)$$

$$3I_2 + 2e^- \rightarrow 2I_3^- \quad (2)$$

We have also performed electrochemical impedance spectroscopic (EIS) measurements on asymmetric dummy cells with Pt and N-GF as the counter electrode, respectively. The obtained Nyquist plots were given in Figure 4d. As can be seen, the first semicircle of N-GF is smaller than that of Pt whereas the second semicircle of N-GF is much larger. From the first semicircle, it was found that both the series resistance (R_s, 21.1 Ω) and the charge-transfer resistance (R_{ct}, 5.6 Ω) of the N-GF electrode are even lower than the corresponding values for the Pt electrode ($R_s = 25.3$ Ω, $R_{ct} = 8.8$ Ω). Because of a lower FF, however, a DSSC based on the N-GF counter electrode showed a slightly lower overall efficiency than its Pt counterpart (Table 1), though they are very comparable. The relatively low FF value for the N-GF-based DSSC is merely a result of the lack of electrode/device optimization.

In summary, we have, for the first time, prepared a nitrogen-doped 3D graphene foam (N-GF) and demonstrated its application as a metal-free electrocatalyst for the reduction of triiodide to replace the Pt cathode in DSSCs, leading to a power conversion efficiency up to 7.07%. This value of efficiency is among the highest efficiencies reported for DSSCs with carbon-based metal-free counter electrodes, comparable to that of a DSSC with a Pt counter electrode constructed under the same condition. Our results indicate that further electrode/device optimization will lead to DSSCs based on the N-GF counter electrode, even outperforming their counterparts with a Pt counter electrode. This work indicates that nitrogen-doped graphene, in particular, and nitrogen-doped carbon nanomaterials, in general, can be used as effective metal-free counter electrodes to replace Pt in high-performance DSSCs.

Received: September 8, 2012
Revised: October 14, 2012
Published online: November 4, 2012

Keywords: carbon · dye-sensitized solar cells · electrochemistry · energy conversion · graphene

[1] B. O'Regan, M. Grätzel, *Nature* **1991**, *353*, 737 – 740.
[2] M. McCune, W. Zhang, Y. Deng, *Nano Lett.* **2012**, *12*, 3656 – 3662.
[3] W. Hong, Y. Xu, G. Lu, C. Li, G. Shi, *Electrochem. Commun.* **2008**, *10*, 1555 – 1558.
[4] H. Han, U. Bach, Y.-B. Cheng, R. A. Caruso, C. MacRae, *Appl. Phys. Lett.* **2009**, *94*, 103102.
[5] T. N. Murakami, S. Wang, Q. Ito, M. K. Nazeeruddin, T. Bessho, I. Cesar, P. Liska, R. Humphry-Baker, P. Comte, P. Pechy, M. Gratzel, *J. Electrochem. Soc.* **2006**, *153*, A2255 – A2261.
[6] R. R. Jia, J. Z. Chen, J. H. Zhao, J. F. Zheng, C. Song, L. Li, Z. P. Zhu, *J. Mater. Chem.* **2010**, *20*, 10829 – 10834.
[7] Z. Yang, T. Chen, R. He, G. Guan, H. Li, L. Qiu, H. Peng, *Adv. Mater.* **2011**, *23*, 5436 – 5439.
[8] J. Han, H. Kim, D. Y. Kim, S. M. Jo, S. Y. Jang, *Acs Nano* **2010**, *4*, 3503 – 3509.
[9] H. Choi, H. Kim, S. Hwang, Y. Han, M. Jeon, *J. Mater. Chem.* **2011**, *21*, 7548 – 7551.
[10] J. D. Roy-Mayhew, D. J. Bozym, C. Punckt, I. A. Aksay, *Acs Nano* **2010**, *4*, 6203 – 6211.
[11] D. W. Zhang, X. D. Li, H. B. Li, S. Chen, Z. Sun, X. J. Yin, S. M. Huang, *Carbon* **2011**, *49*, 5382 – 5388.
[12] C. Mattevi, G. Eda, S. Agnoli, S. Miller, K. A. Mkhoyan, O. Celik, D. Mostrogiovanni, G. Granozzi, E. Garfunkel, M. Chhowalla, *Adv. Funct. Mater.* **2009**, *19*, 2577 – 2583.
[13] D. S. Yu, E. Nagelli, F. Du, L. M. Dai, *J. Phys. Chem. Lett.* **2010**, *1*, 2165 – 2173, and references therein.
[14] S. B. Yang, X. L. Feng, X. C. Wang, K. Müllen, *Angew. Chem.* **2011**, *123*, 5451 – 5455; *Angew. Chem. Int. Ed.* **2011**, *50*, 5339 – 5343.
[15] X. Wang, J. S. Lee, Q. Zhu, J. Liu, Y. Wang, S. Dai, *Chem. Mater.* **2010**, *22*, 2178 – 2180.
[16] L. T. Qu, Y. Liu, J. B. Baek, L. M. Dai, *Acs Nano* **2010**, *4*, 1321 – 1326.
[17] D. S. Yu, Q. Zhang, L. M. Dai, *J. Am. Chem. Soc.* **2010**, *132*, 15127 – 15129.
[18] K. P. Gong, F. Du, Z. H. Xia, M. Durstock, L. M. Dai, *Science* **2009**, *323*, 760 – 764.
[19] Y. Long, C. C. Zhang, X. X. Wang, J. P. Gao, W. Wang, Y. Liu, *J. Mater. Chem.* **2011**, *21*, 13934 – 13941.
[20] Z. S. Wu, S. B. Yang, Y. Sun, K. Parvez, X. L. Feng, K. Müllen, *J. Am. Chem. Soc.* **2012**, *134*, 9082 – 9085.
[21] Z. S. Wu, A. Winter, L. Chen, Y. Sun, A. Turchanin, X. L. Feng, K. Müllen, *Adv. Mater.* **2012**, *24*, 5130 – 5135.
[22] Y. Wang, Y. Y. Shao, D. W. Matson, J. H. Li, Y. H. Lin, *Acs Nano* **2010**, *4*, 1790 – 1798.
[23] Y. C. Lin, C. Y. Lin, P. W. Chiu, *Appl. Phys. Lett.* **2010**, *96*, 133110.
[24] X. L. Li, H. L. Wang, J. T. Robinson, H. Sanchez, G. Diankov, H. J. Dai, *J. Am. Chem. Soc.* **2009**, *131*, 15939 – 15944.
[25] S. Xu, J. Dong, L. Pan, X. Que, Y. Zheng, Y. Shi, X. Wang, *Nano Res.* **2012**, *5*, 361 – 368.
[26] I. Y. Jeon, D. S. Yu, S. Y. Bae, H. J. Choi, D. W. Chang, L. M. Dai, J. B. Baek, *Chem. Mater.* **2011**, *23*, 3987 – 3992.
[27] M. Y. Yen, C. C. Teng, M. C. Hsiao, P. I. Liu, W. P. Chuang, C. C. M. Ma, C. K. Hsieh, M. C. Tsai, C. H. Tsai, *J. Mater. Chem.* **2011**, *21*, 12880 – 12888.
[28] I. K. Moon, J. Lee, R. S. Ruoff, H. Lee, *Nat. Commun.* **2010**, *1*, 73.
[29] Y. Xue, H. Chen, D. Yu, S. Wang, M. Yardeni, Q. Dai, M. Guo, Y. Liu, F. Lu, J. Qu, L. Dai, *Chem. Commun.* **2011**, *47*, 11689 – 11691, and references therein.

